

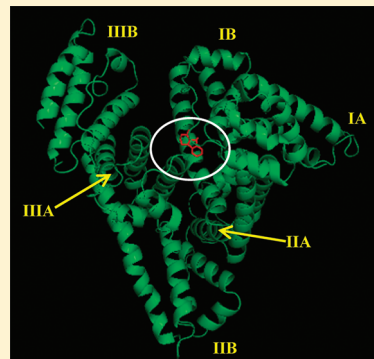
# Modulation of Prototropic Activity and Rotational Relaxation Dynamics of a Cationic Biological Photosensitizer within the Motionally Constrained Bio-environment of a Protein

Bijan Kumar Paul and Nikhil Guchhait\*

Department of Chemistry, University of Calcutta, 92 A. P. C. Road, Calcutta-700009, India

Supporting Information

**ABSTRACT:** The present work describes the interaction of a promising cancer cell photosensitizer, harmane (HM), with a model transport protein, Bovine Serum Albumin (BSA). The studied molecule of interest (HM) belongs to the family of naturally occurring fluorescent drug-binding alkaloids, the  $\beta$ -carbolines. A combined use of steady-state and time-resolved fluorescence techniques is applied to follow and characterize the binding interaction. The polarity-dependent prototropic activity of HM is found to be responsible for the commendable sensitivity of the probe to the protein environments and is distinctly reflected on the emission profile. Steady-state fluorescence anisotropy study reveals the impartation of a considerable degree of motional restriction on the drug molecule as a result of binding to the protein. Contrary to the single-exponential nature of fluorescence anisotropy decay of HM in aqueous buffer, they are found to be biexponential in the protein environment. The rotational relaxation dynamics of HM within the protein has been interpreted on the lexicon of the *Two-Step and Wobbling-in-Cone* model. The probable binding location for the cationic drug is found to be the hydrophilic binding zone of BSA, i.e., domain I (characterized by a net negative charge). The AutoDock-based blind docking simulation has been explored for evaluating an unbiased result of the probable interaction site of HM in the protein. To unfold the effect of binding of the drug on the secondary structural content of the protein, circular dichroism (CD) spectroscopy has been exploited to see that binding of the drug accompanies some decrease in  $\alpha$ -helical content of BSA, and the effect gradually saturates toward a higher drug/protein molar ratio.



## 1. INTRODUCTION

$\beta$ -Carbolines (9H-pyrido[3,4-*b*]indoles) form a family of naturally occurring fluorescent drug-binding alkaloids. The abundance of  $\beta$ -carbolines in nature is quite well-known as they occur in plants, tobacco, and marijuana smoke and are presumably formed in animals as mammalian alkaloids.<sup>1–4</sup>  $\beta$ -Carbolines have long been distinguished and recognized for their wide expanse of biological properties, which include their functioning as potential monoamine-oxidase (MAO) enzyme inhibitors and their interaction with a considerable number of neurotransmitters and neuromodulators of the Central Nervous System (CNS).<sup>1,5–7</sup> They are also well-known for their ability to act as intercalating DNA drugs and their cytotoxic properties,<sup>8–11</sup> which can be enhanced upon photoexcitation by long-wave UV radiation.<sup>1,12–14</sup> Such an ample range of biological activities surrounding  $\beta$ -carbolines has played a pivotal role in forming the nucleus of research to investigate the interaction of these derivatives with biological receptors. Additionally, the novel biological application of  $\beta$ -carbolines in the form of photosensitizer to fungi, viruses, bacteria, etc. is an immensely important topic of research in medical science, the photodynamic therapy (PDT).<sup>15–17</sup>  $\beta$ -Carbolines are reported to be effective in producing singlet oxygen which is detrimental to cancerous, malignant cells.<sup>18,19</sup>

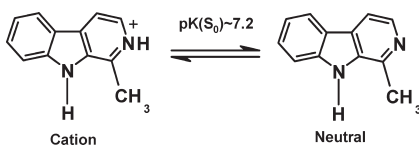
The present study is focused on an endeavor to explore the important and pertinent issue of binding interaction of the biological photosensitizer harmane (HM) (Scheme 1) with a model transport protein, bovine serum albumin (BSA). Serum albumins are abundantly found in blood plasma and belong to one of the most widely studied categories. They function as carriers for numerous exogenous and endogenous compounds in the body. The primary structure of BSA is composed of 583 amino acid residues and is characterized by low tryptophan content along with a high content of cystine, stabilizing a series of nine loops. The secondary structure of serum albumins has 67% of helix of six turns and 17 disulfide bridges.<sup>20–22</sup> The tertiary structure is composed of three domains I, II, and III, and each domain is constituted of two subdomains A and B.<sup>20,21</sup> BSA displays approximately 80% sequence homology and a repeating pattern of disulfides, which are strictly conserved. BSA contains two tryptophan residues, Trp-134 and Trp-212, of which the former is located in hydrophilic subdomain IB and the latter in hydrophobic subdomain IIA.<sup>21</sup> The protein BSA is known to exhibit a very high conformational adaptability to a large variety

**Received:** February 16, 2011

**Revised:** July 1, 2011

**Published:** July 26, 2011

**Scheme 1. Schematic of the Cation  $\rightleftharpoons$  Neutral Prototropic Equilibrium in HM<sup>2b</sup>**



of ligands.<sup>23–25</sup> Furthermore, albumins play instrumental roles in drug deposition and maintenance of colloid-blood pressure in the body.<sup>26</sup>

The present program is designed to focus on deciphering the binding interaction of the biological photosensitizer, HM, with BSA by means of both steady-state and time-resolved fluorescence techniques. The polarity-dependent prototropic transformation in HM has been the actuating tool in the purpose. The interaction of  $\beta$ -carbolines with biological receptors is a field of research which still promises viability to significant expansion. Additionally, the studied  $\beta$ -carboline derivative HM has remained comparatively underutilized in these studies.<sup>27</sup> An attempt is also undertaken to unravel the effect of drug binding on the protein secondary structure to rationalize the applicability of the drug molecule as a therapeutic agent. The binding location of the drug within the protein has been explored based on AutoDock-based “blind docking” strategy and is substantiated from experimental findings. Furthermore, the commendable sensitivity of the photophysical properties of HM toward the microheterogeneous environments of the protein has been utilized as a probe for efficient mapping of chaotrope-induced protein unfolding.

## 2. EXPERIMENTAL SECTION

**2.1. Materials.** Harmane (HM, Scheme 1) was purchased from Aldrich Chemical Co., USA, and used as received. Tris buffer was purchased from SRL, India, and 0.01 M Tris-HCl buffer of pH 7.4 was prepared. Bovine Serum Albumin (BSA) from SRL, India, was used as supplied. Potassium iodide and hydrochloric acid from E-Merck and 1,4-dioxane (UV Spectroscopic grade) from Spectrochem, India, were used as supplied. Triple distilled water was used for the preparation of all solutions. The solvent appeared visually transparent, and its purity was also tested by running the fluorescence spectra in the studied wavelength range.

**2.2. Instrumentation and Methods.** The absorption and emission spectra were acquired on a Hitachi UV-vis U-3501 spectrophotometer and Perkin-Elmer LS-55 fluorimeter, respectively. In all measurements, concentration of HM was maintained at 2.0  $\mu$ M to avoid aggregation and reabsorption effects. Experiments have been carried out at an ambient temperature of 25 °C, unless otherwise specified. Only freshly prepared solutions were used for spectroscopic measurements. For spectral background corrections, a similar set of solutions in increasing BSA concentration was prepared except that the probe was omitted.

Fluorescence quantum yield ( $\Phi_f$ ) was determined using recrystallized anthracene as the secondary standard ( $\Phi_f = 0.27$  in methanol) using the following equation<sup>28</sup>

$$\frac{\Phi_S}{\Phi_R} = \frac{A_S}{A_R} \times \frac{(Abs)_R}{(Abs)_S} \times \frac{n_S^2}{n_R^2} \quad (1)$$

where  $A$  terms denote the fluorescence area under the curve; “Abs” denotes absorbance;  $n$  is the refractive index of the medium;  $\Phi$  is the fluorescence quantum yield; and subscripts “S” and “R” stand in recognition of respective parameters for the studied sample and reference, respectively.

Steady-state anisotropy measurements were carried out using a Perkin-Elmer LS-55 spectrofluorimeter. The steady-state anisotropy is defined as<sup>27–29</sup>

$$r = \frac{(I_{VV} - G \cdot I_{VH})}{(I_{VV} + 2G \cdot I_{VH})} \quad (2)$$

$$G = \frac{I_{HV}}{I_{HH}} \quad (3)$$

in which  $I_{VV}$  and  $I_{VH}$  are the emission intensities when the excitation polarizer is vertically oriented and the emission polarizer is oriented vertically and horizontally, respectively.  $G$  is the correction factor.

Fluorescence lifetimes were measured by a Time-Correlated Single Photon Counting (TCSPC) spectrometer using nanoLED (IBH, U.K.) as the light source at 340 nm to trigger the fluorescence of HM, and the signals were collected at the magic angle of 54.7°. The observed fluorescence intensities were fitted by using a nonlinear least-squares fitting procedure to a function ( $X(t) = A + \int_0^t E(t')R(t-t')dt$ ) comprising the convolution of the IRF ( $E(t)$ ) with a sum of exponentials ( $R(t) = \sum_{i=1}^N B_i e(-t/\tau_i)$ ) with pre-exponential factors ( $B_i$ ), characteristic lifetime ( $\tau_i$ ), and a background ( $A$ ). Relative contribution of each component was obtained from a single- or triexponential fitting and is finally expressed by the following equation

$$\alpha_n = \frac{B_n}{\sum_{i=1}^N B_i} \quad (4)$$

The mean (average) fluorescence lifetimes for the decay curves were calculated from the decay times and the relative contribution of the components using the following equation<sup>28,29</sup>

$$\langle \tau_f \rangle = \frac{\sum_i \alpha_i \tau_i^2}{\sum_i \alpha_i \tau_i} \quad (5)$$

The excellence of the fits was judged by  $\chi^2$  criteria and visual inspection of the residuals of the fitted function to the data.

For time-resolved fluorescence anisotropy decay measurements, the polarized fluorescence decays for the parallel [ $I_{||}(t)$ ] and perpendicular [ $I_{\perp}(t)$ ] emission polarizations with respect to the vertical excitation polarization were first collected at the emission maxima of the probe. The anisotropy decay function  $r(t)$  was constructed from these  $I_{||}(t)$  and  $I_{\perp}(t)$  decays using the following equation<sup>28</sup>

$$r(t) = \frac{I_{||}(t) - G \cdot I_{\perp}(t)}{I_{||}(t) + 2G \cdot I_{\perp}(t)} \quad (6)$$

$G$  is the correction factor for the detector sensitivity to the polarization detection of the emission.

Circular dichroism (CD) spectra were recorded on a JASCO J-815 spectropolarimeter at 25 °C, using a cylindrical cuvette of 0.1 cm path length. The reported CD profiles are an average of

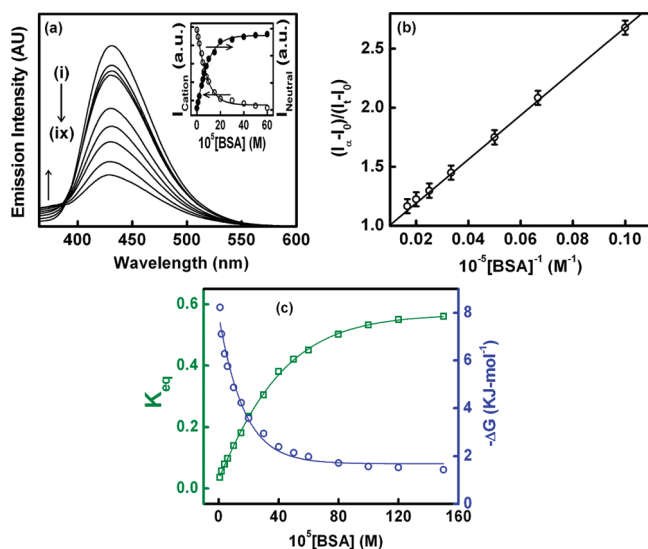


**Figure 1.** (a) Modulation of emission profile of HM with increasing protein concentration ( $\lambda_{ex} = 350$  nm). Curves (i) → (ix) correspond to  $10^5[BSA] = 0, 2, 4, 6, 10, 12, 15, 17$ , and  $20$  M. Inset shows the variation of emission intensities of the cationic (-○-) and neutral (-●-) species of HM as a function of BSA concentration (the solid line provides only a visual guide to the pattern of variation). (b) Benesi–Hildebrand plot of  $(I_{\infty} - I_0)/(I_c - I_0)$  vs  $[BSA]^{-1}$  ( $M^{-1}$ ) for binding of HM to BSA. (c) Variation of equilibrium constant,  $K_{eq}$  (-□-), and free energy change,  $\Delta G$  (-○-), for the equilibrium between neutral and cationic species of HM as a function of BSA concentration (the solid lines provide only a visual guide to the pattern of variation).

four successive scans obtained at 20 nm/min scan rate with an appropriately corrected baseline. The concentration of the protein and the probe during CD measurements is mentioned in the relevant discussion.

**2.3. Docking Study.** The native structure of HSA was taken from the Protein Data Bank having PDB ID: 1AO6. BSA was generated from it by performing necessary additions at the N-terminal as well as some mutations in the required regions, as no PDB is available for BSA.<sup>29c</sup> Docking studies were performed with the AutoDock 4.2 suite of programs which utilizes the Lamarckian Genetic Algorithm (LGA) implemented therein. For docking of HM with BSA, the required file (corresponding to the three-dimensional structure of HM) for the ligand (HM) was created through combined use of Gaussian 03W<sup>30</sup> and AutoDock 4.2<sup>31</sup> software packages. The geometry of HM was first optimized at the DFT//B3LYP/6-31+G\*\* level of theory using the Gaussian 03W suite of programs, and the resultant geometry was read in AutoDock 4.2 software in compatible file format, from which the required file was generated in AutoDock 4.2. At the beginning of the docking study, all water molecules were removed, and hydrogens were added followed by computing Gasteiger charges, as required in the Lamarckian Genetic Algorithm.<sup>31</sup> The grid size was set to 126, 126, and 126 along the  $x$ -,  $y$ -, and  $z$ -axis with 0.558 Å grid spacing; i.e., to recognize the binding site of HM in BSA, blind docking was performed. The AutoDocking parameters used were as follows: GA population size = 150; maximum number of energy evaluations = 250 000; GA cross-over mode = two points. The lowest binding energy conformer was searched out of 30 different conformers for each docking simulation, and the resultant one was used for further analysis.

The PyMoL software package was used for visualization of the docked conformations.<sup>32</sup>

### 3. RESULTS AND DISCUSSION

**3.1. Drug–Protein Binding Interaction: Modulations of Photophysical Properties of the Drug.** The photophysical properties of  $\beta$ -carbolines have long been the subject of considerable interest and have been addressed quite extensively in the literature.<sup>1–14,33</sup> A recent report by Coronilla et al.<sup>1</sup> describes the ground and excited state photophysics of  $\beta$ -carboline and N<sub>9</sub>-methyl- $\beta$ -carboline with particular emphasis on the excited state prototropic activities of the  $\beta$ -carboline derivatives. In analogy to their report and others,<sup>1,27,33</sup> the two absorption band maxima at  $\sim 348$  and  $\sim 370$  nm for HM (which is structurally similar and belongs to the same family of  $\beta$ -carbolines) in aqueous buffer are attributed to the neutral and cationic species, respectively. The prototropic transformations of HM are also substantiated from the pH variation experiments on the absorption and emission profiles of HM as mentioned in the Supporting Information (Section S1, Figures S1 and S2). The absorption spectra of HM are found to undergo no significant modulation upon addition of the protein BSA. These findings are in consensus with a recent report by Mallick et al.<sup>27</sup>

The emission profile of HM exhibits a single, broad, and unstructured band having  $\lambda_{em}^{max}$  at  $\sim 435$  nm in aqueous buffer medium and is ascribed to the emission of cationic species (Scheme 1).<sup>1,27,33</sup> A dramatic modification of the emission profile of HM is observed upon gradual addition of the protein BSA to the aqueous buffer solution of HM (Figure 1a). Increasing protein concentration accompanies a gradual decrease of emission intensity of the band corresponding to the cationic species at  $\sim 435$  nm, with simultaneous development of a new shoulder emission band at  $\sim 380$  nm. A direct comparison with the literature leads us to assign the new blue-shifted emission band to the neutral species of HM (Scheme 1).<sup>1,27,33,34</sup>

Such modulation of the emission profile in the presence of protein is an obvious indication for an enormous modification of the microenvironment in the immediate vicinity of the drug in protein environments compared to those in the bulk aqueous buffer phase. In fact, the present observations as illustrated in Figure 1a can be paralleled to the photophysical properties of HM in a varying composition of dioxane–water mixture to be discussed in a forthcoming section. A gradual decrease of the medium polarity (increase in the dioxane proportion in the water/dioxane reference solvent mixture) is found to result in a regular depletion of emission intensity of the cationic band ( $\lambda_{em} \sim 435$  nm) with simultaneous enhancement of the neutral band intensity ( $\lambda_{em} \sim 380$  nm). Hence, the protein-induced modification (reduction) of the polarity of the microenvironment of the binding site of the probe (HM) seems to be responsible for the observed emission spectral changes (Figure 1a).<sup>1,27,34</sup> The present set of observations also advocates for the dominant role of medium polarity on the prototropic activities of this drug molecule.<sup>1,33</sup>

The inset of Figure 1a shows the variation of emission intensities of the cationic and neutral species as a function of protein concentration. An initial steep change is found to be followed by the attainment of a plateau region showing its onset at  $[BSA] \approx 20 \times 10^{-5}$  M, probably marking the saturation of interaction between the concerned parties.

**Drug–Protein Binding Equilibrium.** A quantitative assessment for the drug–protein binding interaction can be derived in terms of evaluation of the binding constant ( $K$ ) and the free energy change ( $\Delta G$ ) for the process of drug–protein complexation equilibrium. The knowledge of the binding constant ( $K$ ) is important since its binding ability and subsequent influence on the protein stability will govern the therapeutic efficacy of the drug to a large extent.<sup>27</sup> The quantitative evaluation of  $K$  and  $\Delta G$  rests on an analysis of the emission intensity data using the well-known Benesi–Hildebrand equation.<sup>35</sup> A detailed discussion on the Benesi–Hildebrand equation is avoided here since it is routine and profusely available in the literature.<sup>27–29,35</sup> We thus start with the equation

$$1/\Delta I = 1/\Delta I_{\max} + (1/K[BSA])(1/\Delta I_{\max}) \quad (7)$$

which upon rearrangement gives

$$\frac{(I_{\infty} - I_0)}{(I_t - I_0)} = 1 + (K[BSA])^{-1} \quad (8)$$

in which  $\Delta I = I_t - I_0$  and  $\Delta I_{\max} = I_{\infty} - I_0$ , and  $I_0$ ,  $I_t$ , and  $I_{\infty}$  are the emission intensities, respectively, in the absence of BSA, at intermediate concentration of BSA, and at the level of saturation of interaction. Thus, an analysis of the fluorescence data on eq 8 paves the way for simplistic mapping of the spectroscopic modulations on a quantitative scale through estimation of binding parameters and stoichiometry of the HM:BSA complex. As seen in Figure 1b, the plot of  $(I_{\infty} - I_0)/(I_t - I_0)$  vs  $1/[BSA]$  ( $M^{-1}$ ) abides by a linear regression indicating the formation of a 1:1 stoichiometry between HM and BSA (the so-mentioned quantitative analysis of fluorescence data has been framed by considering the cationic fluorescence of the drug). A quantitative estimate of the extent of binding, i.e., the binding constant ( $K$ ), is determined from the slope of the Benesi–Hildebrand plot, and the calculated value is  $K (\pm 10\%) = 6.3 \times 10^3 M^{-1}$ . The free energy change for this process of complexation is thus determined to be  $\Delta G = -RT \ln K = -22.59 \text{ kJ mol}^{-1}$  ( $T$  = experimental temperature = 298 K). A high  $K$  value indicates strong binding between probe and protein BSA, and the favorable process of complexation is dictated by the negative free energy change. The values obtained for  $K (\pm 10\%)$  and  $\Delta G$  are found to be in excellent accord with literature reports for probe–protein complexation equilibria.<sup>22,27,29,36</sup>

**Cation  $\rightleftharpoons$  Neutral Equilibrium.** An understanding of the equilibrium between the neutral and cationic species of HM (Cation  $\rightleftharpoons$  Neutral) and its modulation in proteinous medium can be deduced from the equilibrium constants and free energy changes at various concentrations of the protein. Under the assumption that the fluorescence intensities of the neutral and cationic species of HM are proportional to concentrations of respective species, the equilibrium constant ( $K_{eq}$ ) can be represented as  $K_{eq} = [\text{Neutral}]/[\text{Cation}] = I_{\text{Neutral}}/I_{\text{Cation}}$  and hence the free energy change corresponding to the equilibrium as  $\Delta G = -RT \ln K_{eq}$ . The variation of  $K_{eq}$  and  $\Delta G$  with increasing BSA concentration is displayed in Figure 1c which dictates that the equilibrium is progressively shifted toward the neutral form with increasing protein concentration. The result can be treated as a reflection of the reduced polarity of the binding site of the drug inside the protein cavity compared to that of the bulk aqueous buffer phase and hence substantiates the aforesaid arguments. This result is reinforced in a forthcoming section.

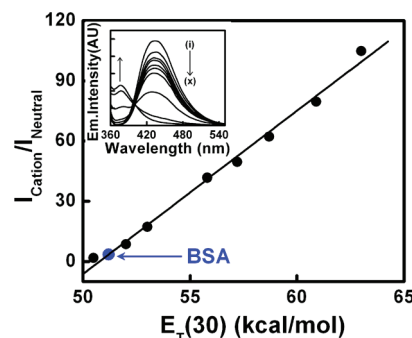


**Figure 2.** Plot of variation of relative emission intensities of the cationic to neutral species of HM ( $I_{\text{Cation}}/I_{\text{Neutral}}$ ) as a function of polarity equivalent parameter,  $E_T(30)$ , of reference solvent mixtures of water–dioxane. Polarity of the binding site of the drug in the protein environment is indicated. Inset shows the emission profile of HM in varying compositions of water–dioxane mixture ( $\lambda_{\text{ex}} = 350 \text{ nm}$ ). Curves (i)  $\rightarrow$  (x) correspond to % dioxane (by volume) = 0, 10, 20, 30, 40, 50, 60, 70, 80, and 90.

**3.2. Polarity of the Drug (HM) Microenvironment.** The precise determination of microscopic polarity of biological and biomimicking assemblies is an important goal in biological and biochemical research. Environment-sensitive photophysical properties of fluorescent probes have been employed to serve this purpose for a couple of decades.<sup>27–29,36</sup> The local polarity of the drug binding site of the protein can be estimated by comparing the spectral properties of the drug in the environment with those in pure solvent or a solvent mixture of known polarity. Although the polarity of a microheterogeneous environment is not exactly the same as that of a homogeneous fluid, a relative estimate of the micropolarity around the fluorophore generally yields reliable results.<sup>27–29,36</sup> In this section, the medium polarity-dependent emission behavior of HM has been exploited to estimate the micropolarity of its immediate surroundings within the protein environment. In Figure 2, a calibration curve has been constructed by plotting the ratio of emission intensities of the cationic and neutral species of HM in varying compositions of a water–dioxane mixture of known polarity as a function of polarity equivalent parameter,  $E_T(30)$ .<sup>27–29,36,37</sup> Extrapolation of the numerical magnitude of the ratio,  $I_{\text{Cation}}/I_{\text{Neutral}}$ , for HM in  $30 \times 10^{-5} M$  BSA leads to a polarity value of 51.23 on the  $E_T(30)$  scale for the microheterogeneous system. Thus, the microenvironment around the drug binding site in the protein backbone is considerably hydrophobic in comparison to the bulk aqueous buffer phase ( $E_T(30)/\text{kcal mol}^{-1} = 63.1^{37}$ ) and hence substantiates the observations reported in the foregoing section (vide Figure 1).

The inset of Figure 2 reveals that a gradual decrease in medium polarity (executed by increasing the dioxane proportion in the water/dioxane mixture) is associated with a progressive enhancement of emission intensity of the neutral species together with a reduction of the same on the cationic counterpart. The consequent increasing degree of destabilization of the cationic species with decreasing medium polarity corroborates this observation. An enhanced neutral to cationic fluorescence yield in the protein environments from that in the bulk aqueous phase (Section 3.1, Figure 1) thus signals toward a less polar microenvironment surrounding the probe in the protein.<sup>27–29,36</sup>

Herein, during construction of the calibration curve (Figure 2), we have emphasized the use of the ratio  $I_{\text{Cation}}/I_{\text{Neutral}}$  rather than

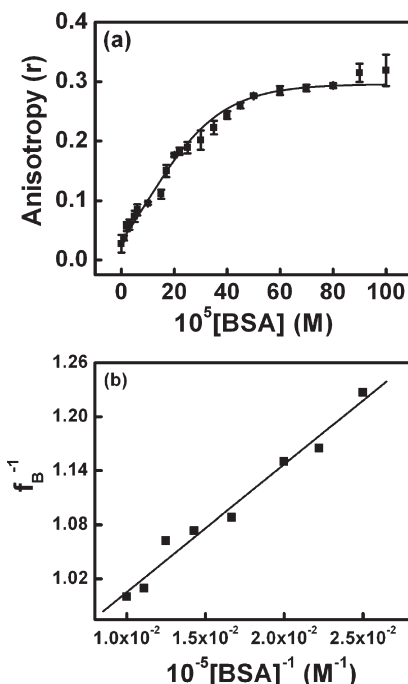


**Figure 3.** (a) Variation of steady-state fluorescence anisotropy ( $r$ ) of HM ( $\lambda_{\text{ex}} = 350 \text{ nm}$ ,  $\lambda_{\text{monitored}} = \lambda_{\text{em}}^{\max}$ ) against increasing concentration of the protein BSA. (Each data point is an average of 15 individual measurements. The error bars are within the symbols if not apparent. The solid line provides only a visual guide to the pattern of variation.) (b) Plot of  $f_B^{-1}$  vs  $[BSA]^{-1}$  ( $M^{-1}$ ) for evaluating the binding constant for HM–BSA binding interaction from anisotropy data (see text for elaboration of the terms).

using only the cationic or only neutral band intensity since the overall photophysics of HM is dictated through spectral characteristics of both the species.

**3.3. Steady-State Fluorescence Anisotropy.** The microenvironment of the probe molecule is governed by its precise location in complex molecular assembly. Any modulation in the rigidity of the surrounding environment of the fluorophore will be reflected through anisotropy values. The so-called environment induced motional restriction on the mobility of the probe in proteinous medium<sup>27–29,36</sup> is manifested through anisotropy variation and thereby furnishes clues to assess the location of the probe within the complex biological environments. In the present case, the fluorescence anisotropy of HM (Figure 3a;  $\lambda_{\text{ex}} = 350 \text{ nm}$  and  $\lambda_{\text{monitored}} = \lambda_{\text{em}}^{\max}$ ) exhibits specific variation as a function of the protein concentration. An initial steep rise in the anisotropy value implies the increasing degree of motional restriction on the probe molecules upon binding to the protein up to  $[BSA] \approx 40 \times 10^{-5} \text{ M}$ , which is then followed by a gradual saturation.

The variation of anisotropy of the fluorophore after binding to the protein is governed by the simultaneous operation of several factors like: (i) the three-dimensional shape and motions of the protein and drug–protein complex and (ii) the global Brownian tumbling of the drug–protein complex.<sup>27,28,36,38</sup> Naturally, the overall dimension of the drug–protein complex will be much larger compared to the unbound fluorophore per se and will, in turn, ascertain a significant reduction on the overall tumbling motion of the former leading to an increase in anisotropy.<sup>27–29,36,38</sup>

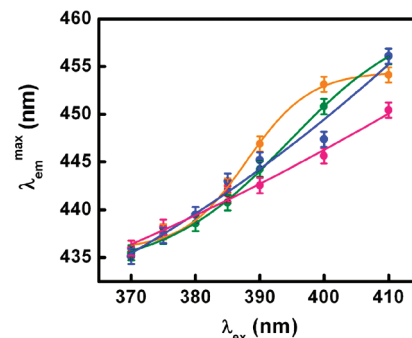


**Figure 4.** REES spectra in terms of variation of emission maxima ( $\lambda_{\text{em}}^{\max}$  (nm)) of HM as a function of excitation wavelength ( $\lambda_{\text{ex}}$  (nm)) at several defined concentrations of BSA.  $10^5 [BSA]$  (M) = 10 (pink), 15 (orange), 50 (green), 60 (blue). The solid lines provide only a visual guide to the pattern of variation.

**Determination of the Binding Constant from Steady-State Anisotropy.** The applicability of anisotropy measurements has been extended in this section to determination of the probe–protein binding constant independently. The details of the method are described elsewhere<sup>39</sup> and are thus avoided here. The determination of the binding constant ( $K$ ) is based on the following equations

$$\frac{1}{f_B} = 1 + \frac{1}{K[BSA]} \quad (9)$$

$$f_B = \frac{r - r_F}{R(r_B - r) + r - r_F} \quad (10)$$

in which  $f_B$  is the fractional fluorescence contribution from the protein-bound probe and  $r_F$  and  $r_B$  are the anisotropy values corresponding to the free (or unbound) and protein-bound probe, respectively.  $R$  is a correction factor ( $R = I_B/I_F$ , the ratio of intensities measured under the same experimental conditions and instrumental settings as those during anisotropy measurements) which is introduced to take care of the fact that HM undergoes emission intensity modulation upon interaction with BSA. The plot of  $1/f_B$  vs  $1/[BSA]$  (Figure 3b) complies with a linear regression yielding  $K = 7.05 \times 10^3 \text{ M}^{-1}$ . A commendable harmony with the value determined from emission intensity data (Section 3.1) thus not only establishes the reliability of the results but also substantiates the practical applicability and feasibility of the methods employed for estimation of the constant.

**3.4. Wavelength-Sensitive Fluorescence Parameter: The Red-Edge Excitation Effect.** A wavelength-sensitive tool for directly monitoring the environment and dynamics around a fluorophore in a complex biological system and the solvation dynamics in an organized medium is the “Red-Edge Excitation Shift” or REES, i.e., the shifting of the emission maxima to the red end of the spectrum upon shifting of the excitation wavelength to the red end of the absorption spectrum of the fluorophore.<sup>29,40–42</sup> Here we have monitored the dependence of emission maxima of HM on the excitation wavelength in the presence of various concentrations of BSA, and the results are displayed in Figure 4. The occurrence of excitation-wavelength dependence is connected to the presence of ensembles of molecules in the ground state differing in their solvation sites and hence energies.<sup>40–42</sup> Precisely, the operation of REES is subject to the following conditions: (a) There should exist a

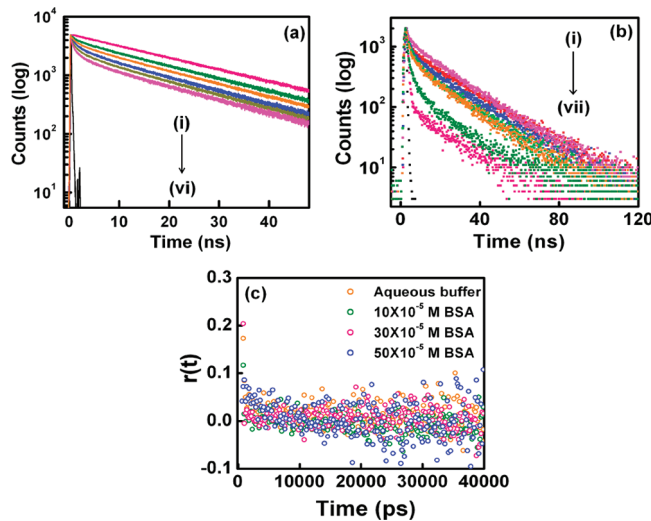


**Figure 5.** (a) Typical time-resolved fluorescence decay profile ( $\lambda_{\text{ex}} = 340 \text{ nm}$ ,  $\lambda_{\text{monitored}} = \lambda_{\text{em max}}$ ) of HM in aqueous buffer and in the presence of increasing protein concentration. Curves (i) → (vi) correspond to  $10^5[\text{BSA}] = 0, 10, 20, 30, 40$ , and  $50 \text{ M}$ . The sharp black profile on the extreme left represents the IRF. (b) Typical time-resolved fluorescence decay profile of HM in various compositions of water–dioxane mixture. Curves (i) → (vii) correspond to volume percentage of dioxane = 10, 30, 40, 50, 60, 70, and 80. The sharp black profile on the extreme left represents the IRF. (c) Representative time-resolved anisotropy decay profiles for HM in various environments as indicated in the figure legend ( $\lambda_{\text{ex}} = 340 \text{ nm}$ ,  $\lambda_{\text{monitored}} = \lambda_{\text{em max}}$ ).

distribution of solute–solvent interaction energy leading to inhomogeneous broadening of the absorption spectra which subsequently will allow the provision of site photoselection of energetically different species. Such inhomogeneous broadening is shown to be particularly significant for molecules having a greater dipole moment in the excited state than in the ground state and is described by a simple expression according to Onsager sphere approximation:<sup>40</sup>  $\Delta\nu = A\Delta\mu\rho^{(-3/2)}(kT)^{(1/2)}$  (here  $A$  is a constant that depends on the dielectric constant of the medium;  $\rho$  is the Onsager cavity radius;  $k$  is the Boltzmann constant; and  $\Delta\mu$  is the change of dipole moment following excitation). However, additional broadening, which can play even a greater role in inhomogeneous broadening of absorption spectra, may be induced by specific interactions of the sort of hydrogen bonding, electrostatic interactions, and so forth.<sup>40–42</sup> (b) Second, the solvent molecules around the fluorophore must be polar, and the solvent reorientation time ( $\langle\tau_{\text{solvent}}\rangle$ ) should be slower or comparable to the fluorescence lifetime ( $\tau_f$ ) of the fluorophore so that unrelaxed fluorescence can give rise to excitation-wavelength-dependent emission behavior.

Figure 4 illustrates that the shift of excitation wavelength from 350 to 410 nm results in a shift of the emission maxima of the probe to the red.<sup>41c</sup> The effect is seen in a general manner for a range of BSA concentrations (with increasing degree of REES as a function of increasing BSA concentration), which suggests that binding of the probe to BSA offers restriction to the rotation of solvent dipoles around the excited fluorophore. Furthermore, given the complex structural architecture of BSA, additional broadening of absorption spectra (as mentioned above) is not unlikely to contribute to the operation of REES in the present case.<sup>29,40–42</sup>

In a nut-shell, the present observations imply that binding of HM to the protein causes considerable restriction to the orientation of solvent dipoles around the excited state fluorophore.

**3.5. Time-Resolved Measurements.** (a) *Time-Resolved Fluorescence Decay.* Fluorescence lifetime measurement serves as a sensitive and faithful indicator for exploring the local environment around a fluorophore.<sup>27–29,36</sup> It also exerts imperative contributions to the understanding of the interactions between the probe and the protein.<sup>27–29</sup> To deduce an elaborate analysis of the scenario, we have monitored the fluorescence lifetime of HM in aqueous buffer medium and in the presence of a series of BSA concentrations. The typical time-resolved fluorescence decay profiles are displayed in Figure 5a, and the fitting parameters are summarized in Table 1a. The drug molecule is found to exhibit a single-exponential decay pattern in bulk aqueous buffer phase with a lifetime of 21.67 ns.<sup>27,43</sup> The data compiled in Table 1a underline that the presence of the protein renders the time-resolved fluorescence decay of the protein-bound probe to be multiexponential when a complicated triexponential function was required to fit the data adequately. Multiexponential decay of fluorescence in the microheterogeneous environment of a protein is not surprising,<sup>27–29,36</sup> but it is often difficult to assign specific mechanistic models to individual decay components (it could even be misleading in cases).<sup>27–29,36,38a</sup> Therefore, it is rational to use the mean (average) fluorescence lifetime of HM for exploiting its behavior within the protein environment, rather than emphasizing individual decay time constants.<sup>27–29,36</sup> A glance at Table 1a reveals that the average lifetime of the probe progressively decreases with increasing protein concentration, whereby it paves a way for assessing the degree of exposure of the probe to aqueous buffer environment. A greater proximity between the lifetime values of the probe in aqueous buffer and protein environments should reflect a greater degree of exposure of the former to the aqueous environment. Thus, the data in Table 1a can be rationalized on the lexicon of strong binding interaction between the probe and the protein resulting in the observed modifications in fluorescence lifetime of HM.<sup>27,28</sup> For the sake of a qualitative comparison, the time-resolved fluorescence decay behavior of HM has also been monitored with varying polarity of the medium, i.e., in varying compositions of water–dioxane reference solvent mixtures as displayed in Figure 5b with the corresponding fitting parameters being compiled in Table 1b (see also Section S3 of Supporting Information).

With a view to delve deeper into the modulations of excited state photophysical properties of the drug within the protein, we have calculated the radiative ( $k_r$ ) and nonradiative ( $k_{nr}$ ) decay rate constants for HM in increasing BSA concentration using the following two equations<sup>28</sup>

$$k_r = \frac{\Phi_f}{\langle\tau_f\rangle} \quad (11)$$

$$k_{nr} = \langle\tau_f\rangle^{-1} - k_r \quad (12)$$

in which  $\Phi_f$  is the fluorescence yield and  $\langle\tau_f\rangle$  is the mean fluorescence lifetime of the cationic species of HM. The photophysical parameters collected in Table 1a unravel a considerable reduction in radiative rate constant ( $k_r$ ) of HM with concomitant enhancement of the nonradiative rate constant ( $k_{nr}$ ) as a function of protein concentration. Thus the lowering of  $\langle\tau_f\rangle$  of HM in the protein environment can be

**Table 1.** (a) Time-Resolved Fluorescence Decay Parameters, Quantum Efficiency ( $\Phi_f$ ), and Radiative ( $k_r$ ) and Nonradiative ( $k_{nr}$ ) Decay Rate Constants for HM in Aqueous Buffer and Protein Environments and (b) Time-Resolved Fluorescence Decay Parameters for HM in Varying Compositions of Water–Dioxane Mixtures

(a) environment	$\tau_1$ (ns)	$\tau_2$ (ns)	$\tau_3$ (ns)	$\alpha_1$ (%)	$\alpha_2$ (%)	$\alpha_3$ (%)	$\chi^2$	$\langle \tau_f \rangle$ (ns)	$\Phi_f$	$k_r \times 10^{-7}$ ( $s^{-1}$ )	$k_{nr} \times 10^{-7}$ ( $s^{-1}$ )
aqueous buffer	21.67 ( $\pm 0.03$ )	—	—	100	—	—	1.09	21.67	0.63	2.91	1.71
$10 \times 10^{-5}$ M BSA	19.9 ( $\pm 0.06$ )	2.75 ( $\pm 0.04$ )	0.65 ( $\pm 0.02$ )	78	11	11	1.05	19.49	0.18	0.92	4.21
$20 \times 10^{-5}$ M BSA	19.16 ( $\pm 0.06$ )	3.02 ( $\pm 0.03$ )	0.72 ( $\pm 0.009$ )	67	15	19	1.09	18.38	0.10	0.54	4.90
$30 \times 10^{-5}$ M BSA	18.43 ( $\pm 0.07$ )	3.29 ( $\pm 0.03$ )	0.79 ( $\pm 0.01$ )	55	18	27	1.12	17.27	0.09	0.52	5.27
$40 \times 10^{-5}$ M BSA	18.07 ( $\pm 0.06$ )	2.83 ( $\pm 0.04$ )	0.64 ( $\pm 0.01$ )	48	20	33	1.13	16.77	0.05	0.30	5.66
$50 \times 10^{-5}$ M BSA	17.71 ( $\pm 0.08$ )	2.37 ( $\pm 0.08$ )	0.49 ( $\pm 0.009$ )	40	22	38	1.14	16.27	0.04	0.25	5.90

(b) % of water (by volume)	$\tau_1$ (ns)	$\tau_2$ (ns)	$\tau_3$ (ns)	$\alpha_1$ (%)	$\alpha_2$ (%)	$\alpha_3$ (%)	$\chi^2$
100	21.67 ( $\pm 0.03$ )	—	—	100	—	—	1.09
90	20.8 ( $\pm 0.05$ )	1.38 ( $\pm 0.03$ )	—	81	19	—	1.12
80	20.2 ( $\pm 0.06$ )	1.6 ( $\pm 0.05$ )	—	81	19	—	1.14
70	19.9 ( $\pm 0.06$ )	1.77 ( $\pm 0.04$ )	—	82	18	—	1.17
60	18.5 ( $\pm 0.08$ )	2.2 ( $\pm 0.03$ )	—	77	23	—	1.16
50	19.4 ( $\pm 0.06$ )	2.09 ( $\pm 0.04$ )	—	51	49	—	1.18
40	18.5 ( $\pm 0.07$ )	4.22 ( $\pm 0.06$ )	1.04 ( $\pm 0.003$ )	68	15	17	1.18
30	17.3 ( $\pm 0.05$ )	3.1 ( $\pm 0.03$ )	0.735 ( $\pm 0.002$ )	86	0.03	11	1.24
20	22.0 ( $\pm 0.08$ )	4.37 ( $\pm 0.04$ )	0.597 ( $\pm 0.003$ )	98	0.9	1.3	1.16

**Table 2.** (a) Dynamic Parameters for Time-Resolved Anisotropy Decay of HM in Aqueous Buffer and Protein Environments and (b) Different Rotational Parameters for HM in Protein Environment as Calculated on the Basis of the Two-Step and Wobbling-in-Cone Model

(a)	$\alpha_{1r}$ environment	$\alpha_{2r}$ (%)	$\tau_{1r}$ (ps)	$\tau_{2r}$ (ns)	$\langle \tau_r \rangle$ (ns)
aqueous buffer	100	—	124 ( $\pm 0.016$ )	—	0.124
$10 \times 10^{-5}$ M BSA	78	22	123 ( $\pm 0.012$ )	9.8 ( $\pm 1.45$ )	2.25
$30 \times 10^{-5}$ M BSA	65	35	125 ( $\pm 0.019$ )	10.0 ( $\pm 1.4$ )	3.58
$50 \times 10^{-5}$ M BSA	54	46	129 ( $\pm 0.019$ )	11.5 ( $\pm 0.019$ )	5.36
$70 \times 10^{-5}$ M BSA	48	52	130 ( $\pm 0.02$ )	13.5 ( $\pm 0.017$ )	7.08
$80 \times 10^{-5}$ M BSA	46	54	131 ( $\pm 0.022$ )	13.7 ( $\pm 0.025$ )	7.45

(b)	$\tau_D$ environment	$\tau_W$ (ns)	$\theta$ (deg)	$D_W \times 10^{-9}$ ( $s^{-1}$ )	$\eta_m$ (cP)
$10 \times 10^{-5}$ M BSA	11.94	124	0.47	53.78	2.33
$30 \times 10^{-5}$ M BSA	12.25	126	0.59	45.91	1.19
$50 \times 10^{-5}$ M BSA	14.57	130	0.67	40.45	0.95
$70 \times 10^{-5}$ M BSA	17.94	131	0.72	36.87	0.81
$80 \times 10^{-5}$ M BSA	18.29	132	0.73	36.13	0.77

attributed to the enhanced nonradiative rates. Further, these data reflect a strong corroboration to the observed modifications on the steady-state emission profile of HM (vide Figure 1, Section 3.1) in the sense that a decrease of  $k_r$  with simultaneous increase of  $k_{nr}$  for the cationic fluorescence of HM in protein environment can be intertwined with lowering of emission

intensity of the cationic species of HM (Figure 1) as a function of the protein concentration.

(b). *Time-Resolved Fluorescence Anisotropy Decay.* To obtain further insight into the microenvironment around the drug, a time-resolved fluorescence anisotropy decay study has been performed for HM in aqueous buffer and in the presence of the protein. The time-dependent decay of fluorescence anisotropy is a sensitive tool for gathering information about the rotational motion and/or rotational relaxation of the fluorophore in an organized assembly.<sup>28,38a,44,45</sup> The typical anisotropy decay profile of HM in aqueous buffer as well as protein environment is presented in Figure 5c, and the corresponding fitting parameters are collected in Table 2a. The fluorophore is seen to exhibit single exponential anisotropy decay (with a reorientation time of 124 ps) in aqueous buffer, while in protein environments the decay follows a biexponential pattern (with a slow and a fast reorientation time). The observation of a biexponential pattern in the anisotropy decay of HM in BSA with two different correlation times implies the presence of two dynamical processes occurring on different time scales.<sup>28,46</sup> The average rotational correlation time for HM in a defined protein concentration (Table 2a) is found to be less than the fluorescence lifetime in the same (Table 1a), suggesting that the depolarization is essentially complete within the excited state lifetime of the probe in the specified environment.

The functional form of the biexponential anisotropy decay,  $r(t)$ , in protein can be represented as follows<sup>28</sup>

$$r(t) = r_0 \times [\alpha_{1r} \exp(-t/\tau_{1r}) + \alpha_{2r} \exp(-t/\tau_{2r})] \quad (13)$$

in which  $r_0$  is the limiting anisotropy that describes the inherent depolarization of the fluorophore and  $\alpha_{ir}$  is the pre-exponent that provides the fraction of the  $i^{\text{th}}$  rotational relaxation time, i.e.,  $\tau_{ir}$ .

At first glance, the data compiled in Table 2a are found to reflect slowing down of the average rotational correlation time

$\langle\tau_r\rangle$ ) of HM with increasing BSA concentration as compared to that in aqueous buffer phase. This suggests that the probe molecule experiences a motionally restricted environment within the protein.<sup>28,44–47</sup> The average rotational relaxation time has been calculated using the following equation<sup>28,44,45</sup>

$$\langle\tau_r\rangle = \alpha_{1r}\tau_{1r} + \alpha_{2r}\tau_{2r} \quad (14)$$

Time-resolved anisotropy can be employed as a faithful tool to cast light on the distribution and/or location of the probe in the microheterogeneous environment. In principle, several arguments might emanate to account for the observed biexponential anisotropy decay behavior of the probe in protein. First, the short and the long components of anisotropy decay can be argued to be coming from the rotational diffusion of the free (unbound) dye (HM) and the protein-bound dye, respectively. However, the validity of such a proposition is immediately questioned by looking at the reasonably high magnitude of binding constant of the dye with the protein (Sections 3.1, 3.3, and 3.6).<sup>28,44,45,47</sup> Besides, had this proposition been correct, the ratio  $\alpha_{2r}/\alpha_{1r}$  would have been corresponding to the ratio of protein-bound dye to the free.<sup>28,44–46</sup> In course, in verifying the validity of this consideration, we have calculated the ratio of concentration of HM in the protein to that in aqueous buffer phase following the method described in the literature (by Quitevis et al., ref 47), and the value is found to be enormously smaller than the ratio  $\alpha_{2r}/\alpha_{1r}$ .<sup>46</sup> This result explicitly dictates that the observed anisotropy decay in the protein environments can be entrusted only on the dynamics of the protein-bound probe while negating any considerable contribution from the free (unbound) dye.<sup>28,44,46</sup>

Another possible interpretation for the biexponential anisotropy decay can be realized in connection with rotational diffusion of the probe bound to two distinct regions of the protein (viz., hydrophilic and hydrophobic interaction sites in BSA<sup>20a,24</sup>). The docking simulation study (to be discussed in a forthcoming section) advocates in favor of probable location of the cationic probe to be in the hydrophilic binding zone domain I of BSA. Indeed, an appreciable population in the hydrophobic interaction sites (domains II and III<sup>20a,24,29</sup>) of the protein does not seem physically rational for the cationic probe HM.<sup>27</sup> Further, for this proposition to be correct, the coefficients  $\alpha_{1r}$  and  $\alpha_{2r}$  should reflect the relative probabilities of finding the dye in the two sites. From the data gleaned in Table 2a, it is evident that the probability of finding the probe in one interaction site is significantly larger than in the other ( $\alpha_{1r} > \alpha_{2r}$ ).<sup>28,44–46</sup>

The aforementioned possibilities are hence invalidated, and the results appear to be in consensus with numerous studies in the literature.<sup>28,38a,44–47</sup> The observed biexponential decay can thus be rationalized in terms of the probe undergoing different kinds of rotational motions in protein environment.<sup>28,38a,44–47</sup> This sort of an observation is often interpreted in light of the well-known *two-step and wobbling-in-cone* model, according to which the fluorescence depolarization can be the result of three independent motions: (a) wobbling of the probe ( $r_W(t)$ ) with a time constant  $\tau_W$ , (b) translational motion of the probe ( $r_D(t)$ ) along the surface of the protein with time constant  $\tau_D$ , and (c) overall rotation of the protein ( $r_P(t)$ ) with a time constant  $\tau_P$ .<sup>28,38a,44–47</sup> The involvement of several kinds of motion leads to deviation of the decay of rotational function,  $r(t)$ , from a single exponential pattern. The so-obtained biexponential decay of  $r(t)$  can thus be ascribed to the interplay of all these motions. Calculation of various rotational parameters on the basis of the two-step and wobbling-in-cone model is described in detail in the

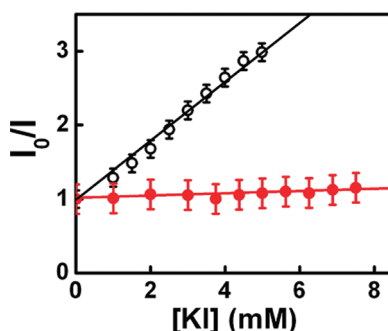


Figure 6. Stern–Volmer plots for fluorescence quenching of HM by potassium iodide in various conditions such as HM in aqueous buffer (-○-) and BSA-bound HM (-●-).

Supporting Information (Section S2), and the dynamical parameters are compiled in Table 2b. The summary of the results is described as follows. The condition  $\tau_P \gg \tau_{2r}$  implies that the slower component  $\tau_{2r}$  essentially represents  $\tau_D$ , suggesting that lateral diffusion comprises an important component in the anisotropy decay of the probe. The data compiled in Table 2a and b clearly reflect that  $\tau_D$  and  $\tau_{2r}$  values are reasonably close to each other. At the same time, an increasing magnitude of the order parameter from 0.47 in  $10 \times 10^{-5}$  M BSA to 0.73 in  $80 \times 10^{-5}$  M BSA is consistent with the idea of increasing degree of motional restriction imposed on the probe. This is further manifested in decreasing value of the semicone angle  $\theta$  with increasing protein concentration (i.e., the treatment of the so-obtained rotational dynamical parameters under the provision of the two-step and wobbling-in-cone model is found to faithfully indicate an increasing degree of motional restriction imposed upon the probe molecule in the protein environment with respect to the bulk aqueous phase). The calculated wobbling diffusion coefficient ( $D_W$ ) (eq S9 of Supporting Information) for the probe in the protein environment is also listed in the table (Table 2b). Also, the rotational dynamical parameters are subsequently exploited to calculate the microviscosity in the immediate vicinity of the probe within the protein (Table 2b). At the same time, that the calculated viscosity for aqueous buffer (1.08 cP) is reasonably close to the reported value provides a strong basis to establish the reliability of our experimental findings and applicability of the method for calculation of the parameters. The details of the calculations are specified in the Supporting Information (Section S2, eq S10).

**3.6. Location of the Probe.** The foregoing discussions clearly establish the occurrence of interaction of HM with the protein BSA. The present section is thus designed to explore the very pertinent as well as important issue of assessing the location of the probe in the protein environment. It is, indeed, quite difficult to deduce an idea about the precise location of the extrinsic molecular probe. Nevertheless, insertion of external perturbations to the photophysics of protein-bound HM and a careful monitoring of its response emerged to form the basis for assessing the location of HM in the studied protein.

(a) *Fluorescence Quenching.* In an endeavor to externally modify the fluorescence of protein-bound HM, we adopted the strategy of quenching of fluorescence of the probe by potassium iodide in different environments. This is a simple but efficient strategy for assessing the location of the probe within the protein. The fluorescence quenching of HM with the addition of the quencher ( $I^-$ ) has been followed on the

following Stern–Volmer<sup>28</sup> equation, i.e.

$$\frac{I_0}{I} = 1 + K_{SV}[Q] \quad (15)$$

in which  $I_0$  is the original fluorescence intensity;  $I$  is the quenched intensity of the fluorophore (HM);  $Q$  is the quencher (here KI); and  $K_{SV}$  is the Stern–Volmer quenching constant. The higher the magnitude of  $K_{SV}$ , the more efficient is the quenching, ensuring a greater degree of exposure of the quencher to the probe.<sup>28</sup> The Stern–Volmer plots for iodide ion-induced quenching of HM in various experimental conditions are displayed in Figure 6. The negatively charged  $I^-$  ion is found to be an efficient quencher for HM (Figure 6) corresponding to  $K_{SV} (\pm 10\%) = 436 \text{ M}^{-1}$ . However, on performing the same quenching experiment on the protein-bound probe (with all experimental conditions and instrumental settings conserved and  $[BSA] = 80 \times 10^{-5} \text{ M}$ ), the extent of quenching is found to be significantly reduced to  $K_{SV} (\pm 10\%) = 9.1 \times 10^{-3} \text{ M}^{-1}$  which corresponds to negligible quenching. This scenario is readily understandable since the dye microenvironment within the protein is determined to be more hydrophobic in comparison to the bulk aqueous buffer phase (Section 3.2), which is not unlikely to resist a closer approach of the ionic quencher to the probe. This is reflected in less efficient quenching of HM in the presence of the protein conforming to lower magnitude of the Stern–Volmer quenching constant (apart from this, an additional effect in terms of electrostatic repulsion between the negatively charged quencher and the protein (BSA) may also contribute in lowering the extent of quenching of the BSA-bound probe by KI).

However, with an ionic quencher ( $I^-$  ion) there remains the possibilities of several interactions emanating from differential electrostatic interactions of the quencher with the neutral and cationic species of the fluorophore. Nevertheless, the quenching results may be treated to yield a qualitative picture for the drug–protein interaction. Moreover, the quenching influence of the  $I^-$  ion on the cationic fluorescence of HM is only monitored here to avoid further complicacies. The linearity obtained in the analysis of the observed fluorescence quenching on the Stern–Volmer equation implies the absence of heterogeneity in the observed quenching phenomenon within the experimental conditions employed.<sup>28</sup>

The bimolecular quenching constant ( $k_q$ ) is defined as  $k_q = K_{SV}/\tau_0$  in which  $\tau_0$  is the fluorescence lifetime of the fluorophore in the absence of the quencher.<sup>28</sup> The upper limit of  $k_q$  for the diffusion-controlled quenching phenomenon is  $2 \times 10^{10} \text{ M}^{-1} \text{ s}^{-1}$ .<sup>28</sup> Values of  $k_q$  smaller than the diffusion-controlled value can result from steric shielding of the fluorophore or a low quenching efficiency, while larger values of  $k_q$  than the diffusion-controlled limit usually indicate some type of binding (ground-state complex formation) interaction. Herein, we avoid a detailed discussion on this approach since it is widely accepted and discussed in detail in the standard literature.<sup>28</sup> On the basis of this approach, the value of  $k_q$  for iodide ion-induced quenching of HM in aqueous buffer medium is estimated to be  $k_q = 2.01 \times 10^{10} \text{ M}^{-1} \text{ s}^{-1}$ , which therefore suggests a diffusion-controlled quenching mechanism, while for BSA-bound HM under the presently employed experimental conditions the bimolecular quenching constant is considerably reduced to  $k_q = 4.95 \times 10^5 \text{ M}^{-1} \text{ s}^{-1}$ , conforming to a significant reduction of the quenching efficiency.

(b). Assessment from Micropolarity in the Immediate Vicinity of the Probe. An appreciable overlap between the donor

(tryptophan in BSA) emission spectrum and the acceptor (HM) absorption spectrum led us to look for the possibility of Fluorescence Resonance Energy Transfer (FRET)<sup>28,29c</sup> occurring in the BSA–HM composite system. However, exciting the BSA–HM composite system at the excitation wavelength of the Trp moiety of the protein reveals no signature for the occurrence of FRET. This implies that the probable location of the probe within the protein backbone is such that it is away from the Trp residue. This finding, for argument's sake, may be taken to negate domain III of the protein to be a probable binding site for this drug since it lacks the Trp residue. Moreover, domain III is known to be more hydrophobic than domain I. In one of our previous reports, the micropolarity near domain II was estimated to be 48.44 on the  $E_T(30)$  scale,<sup>29c</sup> while in the present case it appears to be larger ( $E_T(30) = 51.23 \text{ kcal/mol}$ , vide Section 3.2). This is in consensus with the available literature that domain II (which contains Trp 212) is characterized to be more hydrophobic than domain I.<sup>20,21</sup> Therefore, the nonoccurrence of FRET coupled with the micropolarity assessment appears to discard the hydrophobic domain II as a probable binding location site for HM. Also the negatively charged domain I<sup>20,21</sup> (which contains Trp 134<sup>20,21</sup>) is, of course, more likely to be a favorable binding site for the cationic probe HM. However, that no clear evidence for FRET could be detected appears to imply that the probe is probably not located in near vicinity of the Trp moiety. However, the issue of unfavorable orientation of the donor and acceptor dipoles may also be a probability.<sup>28,29c</sup>

(c). Modeling of Drug Binding Site in BSA: Blind Docking Study. To understand the efficacy of a biologically active drug molecule to function as a therapeutic agent, the knowledge of its binding location in the model transport protein environment is very crucial and important. Herein, the drug (HM) binding site in BSA has been explored on the basis of docking simulation performed according to the protocol described in the experimental section (Section 2.4). With an eye to evaluate an unbiased result in this respect, the AutoDock-based blind docking has been employed as the actuating strategy. The strategy of AutoDock-based blind docking includes a search over the entire surface of the protein for binding sites (and simultaneously optimizes the conformations of the peptides<sup>31,48–50</sup>), whereby it indulges in an unbiased result and hence has rightfully been described as "very encouraging" in a recent review<sup>50</sup> and is also receiving enormous attention from various research groups.<sup>31,48,51</sup> The docked pose displayed in Figure 7 reveals domain I of the protein to be the favorable binding site for the drug.<sup>27</sup> This observation is further substantiated by the fact that the principal hydrophobic binding sites in BSA are located in domains II and III, while domain I, characterized by a net negative charge, can serve as an appropriate binding site for cationic probe molecules.<sup>20a,21,24,27–29</sup> The lowest binding energy conformer was searched out of 30 different conformers for each docking simulation, and the resultant one was used for further analysis. As is usual in a blind docking simulation protocol, we obtained a number of binding sites and the corresponding binding constants and free energies.<sup>31,47–50</sup> Compelling evidence for probable binding location of HM in domain I of BSA was derived from the observation that for binding of HM in the hydrophobic binding sites of BSA, i.e., domains II and III, the binding energy and inhibition constant values were quite high in comparison to that for binding in the hydrophilic binding site domain I, whereas binding of HM in domain I is found to be characterized by a favorable binding energy of  $-5.19 \text{ kcal/mol}$  along with a

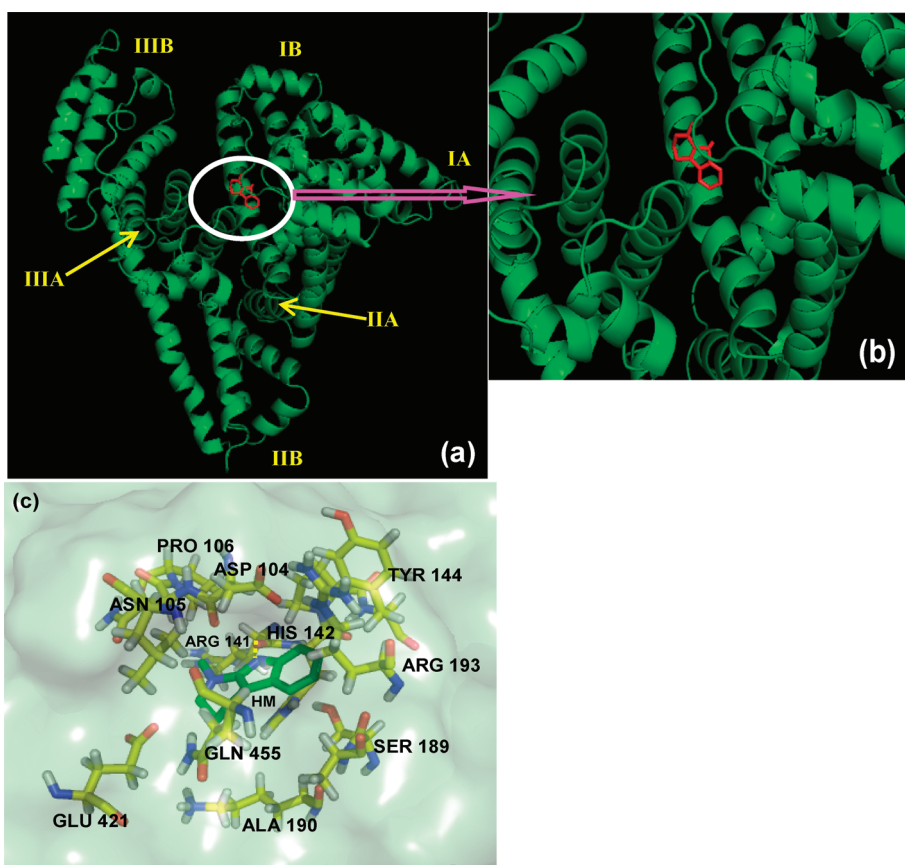


**Figure 7.** (a) View of the docked conformation of the drug HM with the protein BSA. Panel (b) shows the magnified view at the site of interaction of the drug. Panel (c) marks the protein residues in near vicinity of the probe over a molecular surface representation of the protein. Color scheme: white for hydrogen atoms, blue for nitrogen atoms, red for oxygen atoms, and carbon atoms are yellow for protein residues and green for the probe. The pictures have been prepared by the PyMoL software package.<sup>32</sup>

reasonably low magnitude of the inhibition constant, i.e., 158.01  $\mu\text{M}$ . At this juncture it would be imperative to frame a comparison between the experimental results with those obtained from the docking simulation. For this purpose, we bank on the assumption of taking the reciprocal of inhibition constant to be an indicator of the binding constant. With this, the docking results predict a binding constant for the HM–BSA interaction to be = reciprocal of inhibition constant =  $6.33 \times 10^3 \text{ M}^{-1}$  and hence correspondingly the free energy change as  $\Delta G = -RT \ln K = -21.69 \text{ kJ/mol}$  ( $T = 298 \text{ K}$ ); i.e., the results on the HM–BSA binding interaction as revealed from the presently employed blind-docking simulation are in excellent juxtaposition with experimental results (vide Section 3.1 and 3.3), thereby establishing the reliability of the results and substantiating the practical applicability and feasibility of the methods employed for estimation of the parameters. Also Figure 7c marks the protein residues in near vicinity of the probe (e.g., ARG 141, GLN 455, ARG 193, HIS 142, TYR 144, ASP 104, PRO 106, ASN 105) with a possible hydrogen bonding interaction between HIS 142 and the probe molecule (between the carbonyl oxygen ( $-\text{C}=\text{O}$ ) of HIS 142 and the N–H moiety of HM (Figure 7c)). Such hydrogen bonding interaction is not unlikely to contribute in nonradiative decay of the probe within the protein.<sup>28</sup>

### 3.7. Conformation Investigation: Effect of Drug Binding on the Protein Secondary Structure by Circular Dichroism Spectroscopy.

Circular dichroism (CD) spectroscopy has long

been recognized as a robust tool to investigate the secondary structure of a variety of biomolecular systems including proteins. The far-UV CD spectra of BSA exhibit a typical shape corresponding to an  $\alpha$ -helix-rich secondary structure revealing two minima at  $\sim 208$  and  $\sim 222 \text{ nm}$  (Figure 8).<sup>28,29,51</sup> The influence of drug binding interaction on the protein secondary structure has been ascertained by monitoring the far-UV CD spectra of the protein in the presence of increasing concentration of HM, and the results are displayed in Figure 8. Evaluation of such conformational aspects of drug–protein binding is crucial in assessing the efficacy of the drug as a therapeutic agent. As evident from the figure, increasing probe concentration accompanies a small decrease of CD signals at all wavelengths of the far-UV CD spectra of BSA without imposing any shifting of the peak positions. This indicates that binding interaction with HM induces some modification in the secondary structural content of BSA. The lowering in the negative ellipticity points toward a decrease in the  $\alpha$ -helical content which dictates unfolding of the peptide strand even more.<sup>51,52</sup>

Since BSA is a well-recognized transport protein,<sup>20,24,28</sup> a close examination of the modifications to its structural architecture upon binding to various types of substrates naturally demands significance. Thus, to delve deeper into the results of far-UV CD spectra of BSA in the presence of varying HM concentrations (Figure 8), the following analysis of the far-UV CD spectral results has been undertaken.

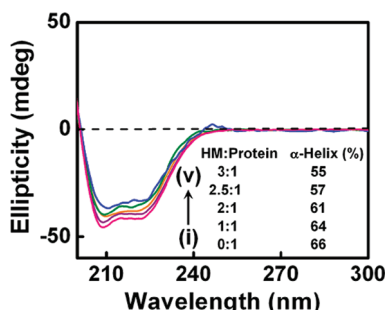


**Figure 8.** Circular dichroism spectra of the protein, BSA ( $4.0 \mu\text{M}$ ), in the presence of varying concentrations of the drug added at  $T = 298 \text{ K}$  in Tris-HCl buffer ( $\text{pH} = 7.40$ ). Percentage change of  $\alpha$ -helix content of the protein at different drug/protein molar ratio is indicated in the figure legend. Error limit in the calculation of %  $\alpha$ -helix is  $\pm 2$ .

The observed CD results are first transformed into mean residue ellipticity (MRE) according to the following equation<sup>52</sup>

$$\text{MRE} (\text{deg cm}^2 \text{ dmol}^{-1}) = \frac{\theta_{\text{obs}}}{C_p n l \times 10} \quad (16)$$

in which  $\theta_{\text{obs}}$  is the observed ellipticity in mdeg;  $C_p$  is the molar concentration of the protein;  $n$  is the number of amino acid residues (583 for BSA<sup>20,24,28</sup>); and  $l$  is the cell path length (here 0.1 cm). The helicity content of the protein is then determined from the calculated MRE values at 222 nm using the following equation<sup>52</sup>

$$\% \alpha\text{-helix} = \frac{-(\text{MRE} - 2340)}{30300} \times 100 \quad (17)$$

The estimated  $\alpha$ -helicity content (eq 17) in free BSA in Tris-HCl buffer ( $\text{pH} = 7.40$  and at  $T = 298 \text{ K}$ ) comes out to be 66 ( $\pm 2\%$ ), which is in reasonable accord with the reported literature.<sup>20,24,28,51,52</sup> The data compiled in Figure 8 inset clearly reveal a perceptible decrease of  $\alpha$ -helicity of the protein with increasing concentration of HM. These results probably indicate partial unfolding of the secondary structure of BSA upon interaction with the drug molecules. The effect was, however, found to be saturated at further drug:protein molar ratio. These results keep consistency with a large volume of literature reports on a variety of ligands (like betulinic acid, chlorogrnac acid, ferulic acid, feruloyl maslinic acid, safranal, retinol, retinoic acid, pentacyclic triterpenoids, and so forth<sup>31,53–56</sup>).

#### 4. SUMMARY AND CONCLUSIONS

The binding interaction of a promising cancer cell photosensitizer, HM, with a model transport protein, BSA, is reported in the present work. The photophysics and rotational relaxation dynamics of the drug are found to be significantly modulated upon binding with the protein. In particular, the modification of polarity-sensitive prototropic activity of HM in the presence of the protein has been assayed on the basis of steady-state and time-resolved emission spectroscopic techniques. Subsequently, such modulations of the photophysics of HM have been exploited to characterize the efficiency and nature of binding, the nature of the microheterogeneous environments around the drug, and micropolarity of the proteinous medium at the binding site. Steady-state anisotropy study is found to strongly complement the efficient binding of the drug into the protein cavity as

derived from steady-state emission data. The REES measurements, on the other hand, evidence for slow reorientation of solvent molecules around the probe in the confined environment. Such characterization of the constrained photophysics of HM within the motionally restricted bioenvironment of the protein is further substantiated from time-resolved study. Various dynamical parameters related to rotational motion of the probe within a motionally constrained protein environment have been estimated using the two-step and wobbling-in-cone model. Subsequently, the binding location of the drug in native BSA has been explored through a blind docking study which reveals domain I (characterized by a net negative charge) to be the favorable binding site for the cationic probe, HM. Further, with an eye to assess the efficacy of the drug to function as a therapeutic agent, the influence of drug binding on the protein secondary structural contents has been evaluated from CD measurements.

#### ■ ASSOCIATED CONTENT

**S Supporting Information.** Information on the effect of pH variation on the absorption and emission spectral properties of HM, calculation of rotational dynamic parameters from the Two-Step and Wobbling-in-Cone model, and time-resolved fluorescence decay behavior of HM in water–dioxane mixture. This material is available free of charge via the Internet at <http://pubs.acs.org>.

#### ■ AUTHOR INFORMATION

##### Corresponding Author

\*Tel: 91-33-2350-8386. Fax: +91-33-2351-9755. E-mail: nguchhait@yahoo.com.

#### ■ ACKNOWLEDGMENT

B.K.P. is grateful to CSIR, Government of India, for a research fellowship. N.G. acknowledges DST, Government of India (Project no. SR/S1/PC/26/2008), for financial assistance. The authors convey their special thanks to Ms. Amrita Sarkar and Professor Dr. Sanjib Bagchi of Indian Institute of Science Education and Research-Kolkata, India, for fluorescence lifetime measurements. We acknowledge the instrumental facilities of Indian Association for the Cultivation of Science, India, for the circular dichroic spectral measurements. Mr. Rajib Pramanik and Prof. Nilmoni Sarkar of Indian Institute of Technology-Kharagpur are gratefully acknowledged for their cooperation with time-resolved fluorescence anisotropy measurement. The cooperation from Ms. A. Gayen and Prof. C. Mukhopadhyay of Department of Chemistry of our university in running the AutoDock 4.2 software program is gratefully acknowledged. We sincerely thank the anonymous reviewers for their meticulous inspection of the manuscript and very constructive suggestions.

#### ■ REFERENCES

- (1) Coronilla, A. S.; Carmona, C.; Munoz, M. A.; Balon, M. *J. Fluoresc.* **2009**, *19*, 1025–1035.
- (2) (a) Abramovitch, R. A.; Spencer, I. D. *Adv. Heterocycl. Chem.* **1964**, *3*, 79–207. (b) Wolfbeis, O. S.; Furlinger, E.; Wintersteiger, R. *Montash. Chem.* **1982**, *113*, 509–517.

- (3) Allen, J. R. F.; Holmstedt, B. R. *Phytochemistry* **1980**, *19*, 1573–1582.
- (4) Balon, M.; Munoz, M. A.; Guardado, P.; Hidalgo, J.; Carmona, C. *Trends Photochem. Photobiol.* **1994**, *3*, 117–138.
- (5) Bloom, H.; Barchas, J.; Sandler, M.; Usdin, E. *Progress in Clinical and Biological Research. Beta-carbolines and Tetrahydroisoquinolines*; Alan R. Liss Inc.: New York, 1982; Vol 90.
- (6) Braestrup, C.; Nielsen, M.; Olsen, C. E. *Proc. Natl. Acad. Sci. U.S.A.* **1980**, *77*, 2288–2292.
- (7) Carlini, E. A. *Pharmacol. Biochem. Behav.* **2003**, *75*, 501–512.
- (8) Meester, C. *Mutat. Res.* **1995**, *339*, 139–153.
- (9) Tamura, S.; Konakahara, T.; Komatsu, H.; Ozaki, T.; Ohta, Y.; Takeuchi, H. *Heterocycles* **1998**, *48*, 2477–2480.
- (10) Balon, M.; Munoz, M. A.; Carmona, C.; Guardado, P.; Galan, M. *Biophys. Chem.* **1999**, *80*, 41–52.
- (11) Cao, R.; Peng, W.; Chen, H.; Ma, Y.; Liu, X.; Hou, X.; Guan, H.; Xu, A. *Biochem. Biophys. Res. Commun.* **2005**, *338*, 1557–1563.
- (12) Hudson, J. B.; Towers, G. H. *Pharmacol. Ther.* **1991**, *49*, 81–122.
- (13) Shimoji, K.; Kawabata, H.; Tomita, I. *Mutat. Res.* **1992**, *268*, 287–295.
- (14) Guan, H.; Liu, X.; Peng, W.; Cao, R.; Ma, Y.; Chen, H.; Xu, A. *Biochem. Biophys. Res. Commun.* **2006**, *342*, 894–901.
- (15) (a) Wang, S.; Gao, R.; Zhou, F.; Selke, M. *J. Mater. Chem.* **2004**, *14*, 487–493. (b) Allison, R. R.; Downie, G. H.; Cuenca, R.; Hu, X.-H.; Childs, C. J. H.; Sibata, C. H. *Photodiag. Photodyn. Ther.* **2004**, *1*, 27–42. (c) Levy, J. G. *Semin. Oncol.* **1994**, *21*, 4–10. (d) Dolmans, D. E. J. G. J.; Fukumura, D.; Jain, R. K. *Nat. Rev. Cancer* **2003**, *3*, 380–387.
- (16) Varela, A. P.; Miguel, M. G.; Maçanita, A. L.; Becker, R. S.; Burrows, H. D. *J. Phys. Chem.* **1995**, *99*, 16093–16100.
- (17) Reyman, D.; Pardo, A.; Poyato, J. M. L. *J. Phys. Chem.* **1994**, *98*, 10408–10411.
- (18) Henderson, B.; Dougherty, T., Eds. *Photodynamic Therapy: Basic Principles and Clinical Applications*; Marcel Dekker Inc.: New York, 1992.
- (19) Chae, K. H.; Ham, H. S. *Bull. Korean Chem. Soc.* **1987**, *7*, 478–479.
- (20) (a) He, X. M.; Carter, D. C. *Nature* **1992**, *358*, 209–215. (b) Chakraborty, T.; Chakraborty, I.; Moulik, S. P.; Ghosh, S. *Langmuir* **2009**, *25*, 3062–3074.
- (21) Peters, T. *Serum albumin. Advances in Protein Chemistry*; Academic Press: New York, 1985; pp 161–245, Vol. 37.
- (22) (a) Abou-Zied, O. K.; Al-Shihi, O. I. K. *J. Am. Chem. Soc.* **2008**, *130*, 10793–10801. (b) Abou-Zied, O. K. *J. Phys. Chem. B* **2007**, *111*, 9879–9885.
- (23) Brown, J. R. *Albumin Structure, Function and Uses*; Rosenoer, V. M., Oratz, M., Rothschild, M. A., Eds.; Pergamon Press: Oxford, 1977, 27.
- (24) Carter, D. C.; Ho, J. X. *Adv. Protein Chem.* **1994**, *45*, 153–159.
- (25) (a) Wu, F.-Y.; Ji, Z.-J.; Wu, Y.-M.; Wan, X.-F. *Chem. Phys. Lett.* **2006**, *424*, 387–393. (b) Zhong, D.; Douhal, A.; Zewail, A. H. *Proc. Natl. Acad. Sci. U.S.A.* **2000**, *97*, 14056–1461. (c) Kamal, J. K. A.; Zhao, L.; Zewail, A. H. *Proc. Natl. Acad. Sci. U.S.A.* **2004**, *101*, 13411–13416.
- (26) Pavridge, W. M. *Am. J. Physiol.* **1987**, *252*, 157–164.
- (27) Mallick, A.; Chattopadhyay, N. *Photochem. Photobiol.* **2005**, *81*, 419–424.
- (28) Lakowicz, J. R. *Principles of Fluorescence Spectroscopy*, 3rd ed.; Plenum: New York, 2006.
- (29) (a) Gelamo, E. L.; Tabak, M. *Spectrochim. Acta* **2000**, *56*, 2255–2271. (b) Gelamo, E. L.; Silva, C. H. T. P.; Imasato, H.; Tabak, M. *Biochim. Biophys. Acta* **2002**, *1594*, 84–99. (c) Paul, B. K.; Samanta, A.; Guchhait, N. *J. Phys. Chem. B* **2010**, *114*, 6183–6196.
- (30) Frisch, M. J. et al. *Gaussian 03*, revision B.03; Gaussian, Inc.: Pittsburgh, PA, 2003.
- (31) (a) Morris, G. M.; Goodsell, D. S.; Halliday, R. S.; Huey, R.; Hart, W. E.; Belew, R. K.; Olson, A. J. *J. Comput. Chem.* **1998**, *19*, 1639–1662 and references therein. (b) Hetenyi, C.; van der Spoel, D. *FEBS Lett.* **2006**, *580*, 1447–1450.
- (32) De Lano, W. L. *The PyMOL Molecular Graphics System*; De Lano Scientific: San Carlos, CA, USA, 2002.
- (33) (a) Tomas Vert, F.; Zabala Sanchez, I.; Olba Torrent, A. *J. Photochem.* **1983**, *23*, 355–368. (b) Wolfbeis, O. S.; Furlinger, E.; Wintersteiger, R. *Monatsh. Chem.* **1982**, *113*, 509–517.
- (34) (a) Hayashi, K.; Nagao, M.; Gugimara, T. *Nucleic Acid Res.* **1977**, *4*, 3679–3685. (b) Gonzalez, M. M.; Arnbjerg, J.; Denofrio, M. P.; Erra-Balsells, R.; Ogilby, P. R.; Cabrarizo, F. M. *J. Phys. Chem. A* **2009**, *113*, 6648–6656.
- (35) Benesi, H. A.; Hildebrand, J. H. *J. Am. Chem. Soc.* **1949**, *71*, 2703–2707.
- (36) (a) Singh, R. B.; Mahanta, S.; Guchhait, N. *Chem. Phys. Lett.* **2008**, *463*, 183–188. (b) Ding, F.; Liu, W.; Liu, F.; Li, Z.-Y.; Sun, Y. *J. Fluoresc.* **2009**, *19*, 783–791.
- (37) Reichardt, C. *Chem. Rev.* **1994**, *94*, 2319–2358.
- (38) (a) Bhattacharya, B.; Nakka, S.; Guruprasad, L.; Samanta, A. *J. Phys. Chem. B* **2009**, *113*, 2143–2150. (b) Berezin, M. Y.; Achilefu, S. *Chem. Rev.* **2010**, *110*, 2641–2684.
- (39) Ingersoll, C. M.; Strollo, C. M. *J. Chem. Educ.* **2007**, *84*, 1313–1315.
- (40) Demchenko, A. P. *Luminescence* **2002**, *17*, 19–42.
- (41) (a) Guz, A.; Wasylewski, Z. *J. Protein Chem.* **1994**, *13*, 393–399. (b) Samanta, A. *J. Phys. Chem. B* **2006**, *110*, 13704–13716 and references therein. (c) During REES measurements, meticulous care has been devoted to the selection of excitation wavelength to ensure that the variation of  $\lambda_{ex}$  involves shifting to the red end of the absorption spectra and not merely the absorption maxima. This is a very crucial criterion for REES monitoring.<sup>40</sup>
- (42) (a) Maglia, G.; Jonckheer, A.; Maeyer, M. D.; Frere, J.-M.; Engelborghs, Y. *Protein Sci.* **2008**, *17*, 352–361. (b) *Reviews in Fluorescence*; Geddes, C. D., Lakowicz, J. R., Eds.; Kluwer-Plenum: New York, 2004. The appearance of Leonardo da Vinci's Universal.
- (43) Berg, J. M.; Tymoczko, J. L.; Stryer, L. *Biochemistry*, 5th ed.; Devlin, T. M., Ed.; W. H. Freeman and Company: New York, 2002.
- (44) Garcia-Zubiri, I. X.; Burrows, H. D.; de Melo, J. S. S.; Pina, J.; Monteserin, M.; Tapia, M. J. *Photochem. Photobiol.* **2007**, *83*, 1455–1464.
- (45) Chakraborty, A.; Seth, D.; Setua, P.; Sarkar, N. *J. Chem. Phys.* **2008**, *128*, 204510–204519.
- (46) (a) Paul, B. K.; Guchhait, N. *J. Phys. Chem. B* **2010**, *114*, 12528–12540. (b) Dutt, G. B. *J. Phys. Chem. B* **2005**, *109*, 4923–4928. (c) Dutt, G. B. *J. Chem. Phys.* **2003**, *119*, 11971–11976. (d) Paul, B. K.; Guchhait, N. *J. Colloid Interface Sci.* **2011**, *353*, 237–247.
- (47) Quitevis, E. L.; Marcus, A. H.; Fayer, M. D. *J. Chem. Phys.* **1993**, *97*, 5792–5796.
- (48) Kinosita, K.; Kawato, S.; Ikegami, A. *Biophys. J.* **1977**, *20*, 289–305.
- (49) (a) Schames, J. R.; Hechtnman, R. H.; Siegel, J. S.; Sottriffer, C. A.; Ni, H.; McCammon, J. A. *J. Med. Chem.* **2004**, *47*, 1879–1881. (b) McKenna, C. E.; Kashemirov, B. A.; Upton, T. G.; Batra, V. K.; Goodman, M. F.; Pedersen, L. C.; Beard, W. A.; Wilson, S. H. *J. Am. Chem. Soc.* **2007**, *129*, 15412–15413.
- (50) (a) Hetenyi, C.; van der Spoel, D. *Protein Sci.* **2002**, *11*, 1729–1737. (b) Pineda, O.; Farras, J.; Maccari, L.; Manetti, F.; Botta, M.; Vilarrasa, J. *Med. Chem. Lett.* **2004**, *14*, 4825–4829.
- (51) Campbell, S. J.; Gold, N. D.; Jackson, R. M.; Westhead, D. R. *Curr. Opin. Struct. Biol.* **2003**, *13*, 389–395.
- (52) (a) Moriyama, Y.; Takeda, K. *Langmuir* **2005**, *21*, 5524–5528. (b) Moriyama, Y.; Takeda, K. *Langmuir* **1999**, *15*, 2003–2008. (c) Moriyama, Y.; Watanabe, E.; Kobayashi, K.; Harano, H.; Inui, E.; Takeda, K. *J. Phys. Chem. B* **2008**, *112*, 16585–16589.
- (53) (a) Hu, Y.-J.; Ou-Yang, Y.; Dai, C.-M.; Liu, Y.; Xiao, X.-H. *Biomacromolecules* **2010**, *11*, 106–112. (b) Wu, X.; Narsimhan, G. *Biochim. Biophys. Acta* **2008**, *1784*, 1694–1701.
- (54) (a) Zsila, F.; Bikadi, Z.; Simonyi, M. *Biochem. Pharmacol.* **2003**, *65*, 447–456. (b) Dufour, C.; Dangles, O. *Biochim. Biophys. Acta* **2005**, *1721*, 164–173. (c) Jiang, Y. L. *Bioorg. Med. Chem.* **2008**, *16*, 6406–6414.

(55) (a) Tayyab, S.; Ahmad, B.; Kumar, Y.; Khan, M. M. *Int. J. Biol. Macromol.* **2002**, *30*, 17–22. (b) Sulkowska, A.; Bojko, B.; Rownicka, J.; Pentak, D.; Sulkowska, W. *J. Mol. Struct.* **2003**, *651*, 237–243.

(56) (a) Beauchemin, R.; Nsoukpo-Kossi, C. N.; Thomas, T. J.; Thomas, T.; Carpentier, R.; Tajmir-Riahi, H. A. *Biomacromolecules* **2007**, *8*, 3177–3183. (b) Nsoukpo-Kossi, C. N.; Sedaghat-Herati, R.; Ragi, C.; Hotchandani, S.; Tajmir-Riahi, H. A. *Int. J. Biol. Macromol.* **2007**, *40*, 484–490.